

R245FA TWO-PHASE FLOW CHARACTERISTICS DURING FLOW BOILING IN MICRO-SCALE CHANNELS

Alexandre A. Arcanjo, alexandrearcanjo@gmail.com
Juliano O. de Freitas, juliano_freitas_7@yahoo.com.br
Gherhardt Ribatski, ribatski@sc.usp.br

Department of Mechanical Engineering,
Escola de Engenharia de São Carlos (EESC), University of São Paulo (USP)
Av. Trabalhador SanCarlense 400, Centro, São Carlos, SP, Brazil

Abstract. Measurements of elongated bubble velocity, frequency and length were performed. The tests were run for R245fa evaporating in a stainless steel tube with diameter of 2.32 mm, mass velocities from 100 to 600 kg/m²s and saturation temperatures of 22°C, 31°C and 41°C. The tube was heated by applying a direct DC current to its surface. Images from a high-speed video-camera (8000 frames/s) obtained through a transparent tube just downstream of the heated section were used to determine elongated bubble velocities, frequencies and lengths. The results suggested that the elongated bubble velocity depends on mass velocity, vapor quality and saturation temperature, and is independent of bubble length. The bubble velocity increases with increasing mass velocity and vapor quality and decreases with increasing saturation temperature. Additionally, bubble velocity was correlated as a linear function of the two-phase superficial velocity.

Keywords: flow boiling, elongated bubbles, micro-channel, flow patterns

1. INTRODUCTION

In-tube macro-scale two-phase flow pattern transitions and flow characteristics such as superficial void fraction, liquid film thickness, interfacial waviness, and vapor piston velocity have been targeted by innumerable researchers since the early 40s. These studies were motivated by the fact that heat transfer, pressure drop and the presence of flow instabilities are intrinsically related to the flow configuration and, consequently, the establishment of a good knowledge of the flow characteristics is crucial in order to built reliable heat transfer and pressure drop prediction methods and heat exchanger design tools.

In the late 90s, pushed mainly by the drastic increase in the number of transistors in a microprocessor and its inherent need of dissipating larger amounts of energy, a massive number of papers on single-phase and flow boiling in micro-scale channels has started to come up focusing on the development of heat spreaders capable of dissipating heat fluxes up to 3MW/m² (see Ribatski *et al.* (2007)).

Most of studies on bubble length distribution, velocity and frequency were performed for macro-scale channels and have focused on Taylor bubbles rising in vertical channels. Thus, on contrary to what occurs in horizontal flows in micro-scale channels, in such cases the flow is turbulent and the vertical bubble ascension is favored by buoyancy effects.

By using an optical measurement technique and image processing of high speed films, Thome and co-workers (Agostini *et al.* (2008), Revellin *et al.* (2008a,b)) have measured vapor bubble lengths, L_G , elongated bubble velocities, U_G , and their frequency, f_b , for flow boiling of R134a in micro-scale tubes. Their measurements were performed with tube diameters, D , of 0.509 mm and 0.790 mm, vapor qualities from 2% to 19% and saturation temperature of 30°C. According to their results, the relative elongated bubble velocity (vapor velocity minus the homogeneous flow velocity, U_H) increases with increasing bubble length until a plateau is reached, and also increases with increasing tube diameter and mass velocity. They proposed a semi-analytical model for the vapor velocity written as a function of the bubble length and expressed as:

$$U_G = \frac{D\gamma}{1-0.58/Co} \frac{1-\exp[-(2L_G f)/D]}{2f} + U_H \quad (1)$$

where γ , and Co , the confinement number, are given by:

$$\gamma = \frac{4q}{Dh_{LG}\rho_G} \quad (2)$$

$$Co = \left[\frac{\sigma}{g(\rho_L - \rho_G)D} \right]^{0.5} \quad (3)$$

and f is the vapor friction factor given by $64/Re_G$ and $0.316/Re_G^{0.25}$ for laminar and turbulent flow, respectively.

In the equations above, σ is the surface tension, ρ_L and ρ_G are the liquid and vapor densities, respectively, g is the gravitational acceleration, q is the heat flux and h_{LG} is the latent heat of vaporization. The vapor Reynolds number, Re_G , is given by GD/μ_G where μ_G is the vapor dynamic viscosity.

A model for predicting the collision of elongated bubbles in horizontal micro-scale flows was proposed by Revellin *et al.* (2008b). This model takes into account differences of velocities among elongated bubbles related to distinct bubbles lengths, and the vapor input into the bubbles due to the evaporation process.

Recently, Arcanjo *et al.* (2009) performed experiments for R134a evaporating in a stainless steel tube with diameter of 2.32 mm. They pointed out that the elongated bubble velocity increases with decreasing saturation temperature and increasing vapor quality and mass velocity. Moreover, according to their results the bubble velocity is almost independent of its length. They also found that the elongated bubble frequency passes through a peak with increasing vapor quality from zero and this peak moves to lower vapor qualities with decreasing mass velocity and has its value increased with increasing saturation temperature.

In this study, elongated bubble velocities, frequencies and lengths were determined based on an analysis of high-speed videos. The tests were run for R245fa evaporating in a stainless steel tube with diameter of 2.32 mm, mass velocities, G , from 100 to 600 kg/m²s and saturation temperatures of 22°C, 31°C and 41°C. The flow images were obtained with a high-speed video-camera (8000 frames/s) from a transparent tube just downstream of the heated section.

The present results suggest that the elongated bubble velocity depends on the mass velocity, vapor quality and saturation temperature. The bubble velocity increases with increasing mass velocity and vapor quality and decreases with increasing saturation temperature. The drift flux model with a new flow distribution parameter predicted satisfactorily the present experimental results.

2. EXPERIMENTS

2.1. Test apparatus and experimental procedure

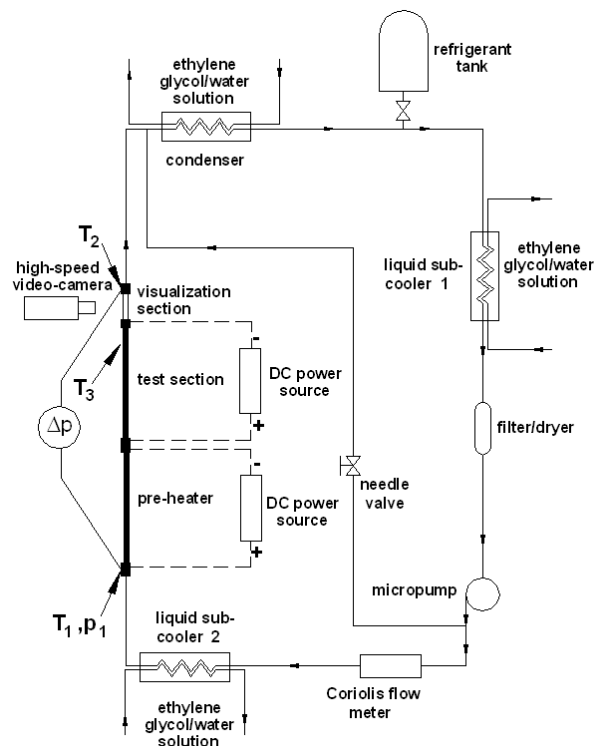


Figure 1. Schematic diagram of the refrigerant circuit.

The experimental setup is comprised of refrigerant and ethylene-glycol circuits. The refrigerant circuit is shown schematically in Fig. 1. It globally comprises a micropump, to drive the working fluid through the circuit, a pre-heater, to establish the experimental conditions at the inlet of the test section, a test section, a visualization section, a condenser to condense the vapor created in the heated sections, and a reservoir. The water-glycol circuit (not shown) is intended to condense and subcool the fluid in the refrigerant circuit. The cooling effect is obtained by a 60% solution of ethylene

glycol/water that operates as intermediate fluid in a system that comprises electrical heaters actuated by PID controllers, 3 water/glycol tanks, heat exchangers and a refrigeration circuit.

In the refrigerant circuit, starting from the subcooler 1, the test fluid flows through the filter to the micropump (self-lubricating without oil). Downstream the micropump, a bypass piping line containing a needle-valve is installed so that together with a frequency controller on the micropump the desired liquid flow rate can be set. There is then a Coriolis mass flow meter and the subcooler 2 to assure that the fluid entering the pre-heater is subcooled. Just upstream the pre-heater inlet, the enthalpy of the liquid is estimated from its temperature T_1 by a 0.25 mm thermocouple within the pipe and its pressure p_1 by an absolute pressure transducer. At the pre-heater, the fluid is heated up to the desired condition at the test section inlet. The pre-heater and the test section are horizontal stainless steel tubes 464 mm long, L , and 2.32 mm ID. Both are heated by applying direct DC current to their surface and are thermally insulated. The power is supplied to them by two independent DC power sources controlled from the data acquisition system. The visualization section is a horizontal fused silica tube with an inner diameter of 2.1mm, a length of 85mm, and is located just downstream to the test section. The pre-heater and the test and visualization sections are connected through junctions made of electrical insulation material and specially designed and machined in such way to match up their ends and keep a smooth and continuous internal surface. Once the liquid leaves the visualization section its temperature T_2 is determined from a 0.25mm thermocouple within the pipe. The corresponding absolute pressure is estimated from a differential pressure transducer that gives the total pressure drop between the pre-heater inlet and the visualization section outlet, Δp . Then, the working fluid is directed to the tube-in-tube type heat exchanger where it is condensed and subcooled by exchanging heat with the anti freezing ethylene glycol aqueous solution. The refrigerant tank operates as a reservoir of the working fluid and is used to control the saturation pressure in the test section in such way that refrigerant is transferred from the refrigerant circuit to the tank when aiming to reduce the operating pressure, and refrigerant is transferred in the opposite way to increase the operating pressure.

2.2. Data reduction

Vapor quality at the inlet of visualization section: The vapor quality was determined by an energy balance over the pre-heater and the test section according to the following equation:

$$x = \frac{1}{h_{LG,out}} \left[\frac{4(P_1 + P_2)}{G\pi D^2} + (h_{L,in} - h_{L,out}) \right] \quad (4)$$

The enthalpy of the liquid at the inlet of the pre-heater, $h_{L,in}$ was estimated based on the measured temperature T_1 and pressure p_1 . The liquid enthalpy and the latent heat of vaporization at the visualization section ($h_{L,out}$ and $h_{LG,out}$, respectively) were estimated based on the fluid temperature measured just downstream the visualization section, T_2 , and assuming saturated state. In Eq. (4), P_1 and P_2 are the electrical power supplied by the DC power sources to the heated sections.

Elongated bubble frequency: From high-speed videos watched in slow motion mode, the bubble frequency was determined by counting the number of bubbles with a length greater than the internal tube diameter, N_b . Then, knowing the total number of frames, N_f , and the recording frame rate (frames/second) FPS , the bubble frequency was calculated as follow:

$$f_b = \frac{N_b}{N_f} FPS \quad (5)$$

Elongated bubble velocity: The velocity was estimated from the number of frames necessary for the elongated bubble nose to go through a distance of 55.55mm. Once determined the number of frames from the high-speed films, the velocity of each bubble, $U_{1,b}$, was calculated according to the following expression:

$$U_{1,b} = 0.05555 \frac{FPS}{N_f} \quad (6)$$

The elongated bubble velocity for each experimental condition, U_G , was calculated as the arithmetic average velocity of 10 bubble samples. This procedure provided relative standard deviations always lower than 5%.

Elongated bubble length: Initially, an image scale, IS , was defined as the ratio between the image length (0.05555m) and the total number of pixels within the image along its horizontal-axis (1280 pixels). Then, if the elongated bubble length is smaller than the image width, the bubble length is calculated as:

$$L_G = IS \cdot N_p \quad (7)$$

Otherwise, if the elongated bubble length is larger than the image width, the bubble velocity is calculated as:

$$L_G = U_{1,b} \cdot \frac{N_f}{FPS} \quad (8)$$

2.3. Experimental validation and uncertainties

Compressible volume instabilities also termed in the literature by “explosive boiling” (see Hetsroni *et al.* (2005) for further details) are a common phenomenon in micro-scale flow boiling. These instabilities can promote severe pressure and temperature oscillations in the flow and seem related to some of discrepancies observed when comparing experimental results from different authors (see Consolini *et al.* (2007)). During the present experimental campaign, such instabilities were not observed and the fluctuations of the fluid temperature and pressure were within the uncertainty range of their measurements.

Single-phase flow experiments were performed in order to assure the accuracy of the estimated vapor quality and evaluate the effective rate of heat transferred to the single phase refrigerant, $(\Delta E/E)$, defined as follow:

$$\left(\frac{\Delta E}{E}\right) = \frac{\left(\left[\frac{\pi D^2}{4}\right] G(h_{out} - h_{in}) - (P_1 + P_2)\right)}{P_1 + P_2} \quad (9)$$

where h_{in} and h_{out} are the refrigerant enthalpies estimated at the pre-heater inlet and just downstream the visualization section, respectively.

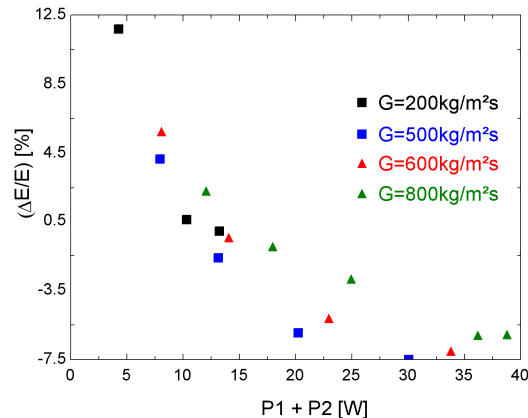


Figure 2. Evaluation of the effective rate of heat transferred to the single-phase flow refrigerant.

Table 1. Uncertainty of measured and calculated parameters.

Parameter	Uncertainty	Parameter	Uncertainty
D	$\pm 20\mu\text{m}$	Δp	± 0.15 kPa
f_b	2 bubbles	P_1, P_2	$\pm 0.8\%$
G	$\pm 0.88\%$	T	± 0.15 °C
L	± 1 mm	U_G	2%
L_b	0.2mm	x	<5%
p	± 4.5 kPa		

As one can see in Fig. 2, the heat losses decrease with increasing the mass velocity with an effective rate of heat transferred to the refrigerant higher than 90% for most of the experimental conditions.

Temperature measurements were calibrated and the temperature uncertainty evaluated according to the procedure suggested by Abernethy and Thompson (1973). Accounting for all instrument errors, uncertainties for the calculated parameter were estimated using the method of sequential perturbation according to Moffat (1988). The experimental uncertainties associated with the sensors and calculated parameters are listed in Tab. 1.

3. EXPERIMENTAL RESULTS AND DISCUSSIONS

Figures 3 and 4 show the effect of saturation temperature and mass velocity on the bubble velocity behavior with increasing vapor quality. As shown by Revellin *et al.* (2008a) and Arcanjo *et al.* (2009), the bubble velocity increases with increasing the vapor quality and mass velocity. Figure 3 also shows that the bubble velocity decreases with increasing saturation temperature. Such a behavior is related to the fact that the vapor/liquid specific volume ratio decreases with increasing saturation temperature and so, the fluid acceleration, inherent to the evaporation process, also decreases.

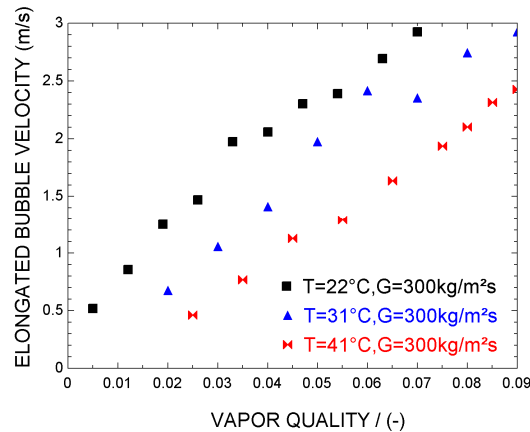


Figure 3. The influence of the saturation temperature on the behavior of elongated bubbles with increasing vapor quality.

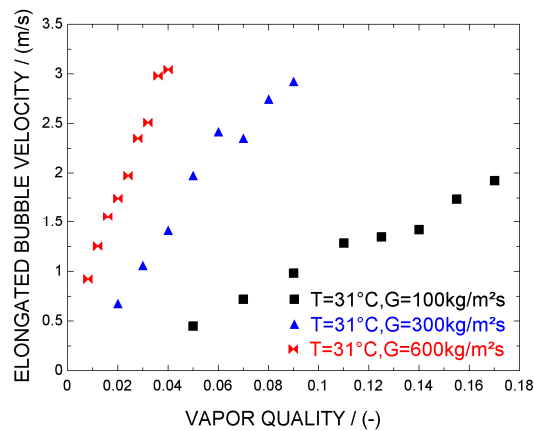


Figure 4. The influence of the mass velocity on the behavior of elongated bubbles with increasing vapor quality.

In the drift flux model proposed by Zuber and Findler (1965) the mean weighted gas velocity is correlated as a linear function of the total superficial velocity, J . So, from this function is possible to obtain the superficial void fraction. According to this model, the slope of the linear function takes into account the non-uniformities of the local void fraction and phase velocity along the channel, and the y-intercept takes into account the weighted mean drift flux velocity. Figure 5 displays the present experimental database in a U_G vs. J chart plus a linear curve-fitting of these data. It is also observed that the drift flux model with a distribution parameter of 1.09 and a drift flux velocity of 0 predicts reasonable well the present database since 79% and 89% of its data was predicted within error bands of $\pm 20\%$ and 30% , respectively. Worst predictions are observed for a saturation temperature of 41°C .

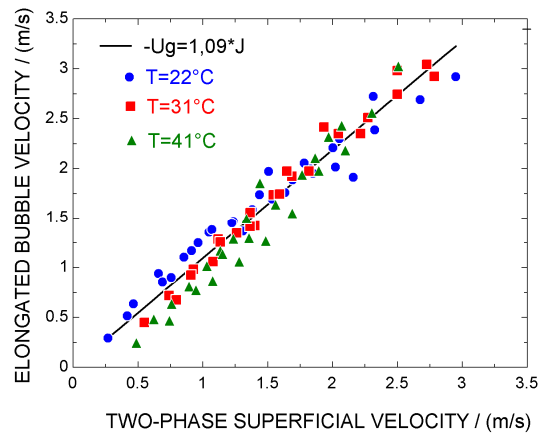


Figure 5. Comparison of the present database and the drift flux model with a new distribution parameter.

Figures 6, 7 and 8 illustrate the effects of mass velocity and saturation temperature on the elongated bubble frequency behavior with increasing vapor quality.

According to Fig. 6, the elongated bubble frequency seems to pass through a peak with increasing the vapor quality from 0. Such a behavior was previously indicated by Thome and coworkers (Revellin and Thome (2007), Revellin *et al.* (2008b)) and Arcanjo *et al.* (2009). In the studies by Revellin and Thome (2007) and Revellin *et al.* (2008b), performed with internal diameter tubes of 0.509mm and 0.790mm, and mass velocities up to 1800kg/m²s, it was observed elongated bubble frequencies up to 900 Hz, thus, values much higher than those observed in this study and by Arcanjo *et al.* (2009). According to Fig. 6 the frequency peak value increases with increasing mass velocity. Such a behavior seems related to the increase of turbulence intensity with mass velocity and its effect on the elongated bubble coalescing and growing processes. It is shown in Fig. 6 that the bubble frequency peak moves to lower vapor qualities with increasing mass velocity. Such a result is expected since, under a condition of greater number of elongated bubbles due to a higher mass velocity, it is probable that bubble coalescing process begins at lower vapor qualities.

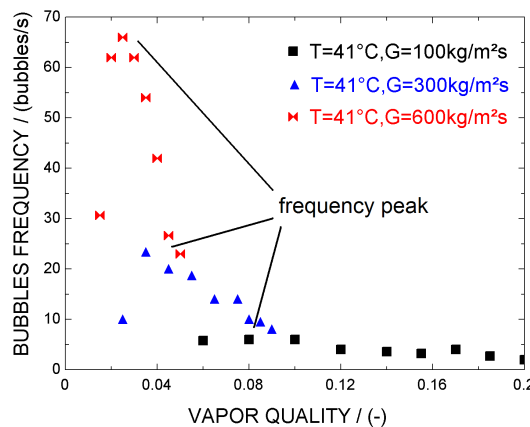


Figure 6. Illustration of the effect of the mass velocity on the elongated bubble frequency.

For a given mass velocity and saturation temperature values Fig. 9 shows that the vapor quality converges asymptotically to a fix value as the bubble length increases. This behavior indicates a vapor quality value at which a transition from elongated bubble to annular flow seems to occur. The plots in Fig. 9 also show that the vapor quality for the flow pattern transition decreases with increasing mass velocity. A negligible effect on the transitional vapor quality by changing the saturation temperature from 21 to 41°C (not shown) was also revealed by the present database. Both behaviors are in agreement with the flow pattern predictions given by the micro-scale flow pattern predictive method proposed by Felcar *et al.* (2007).

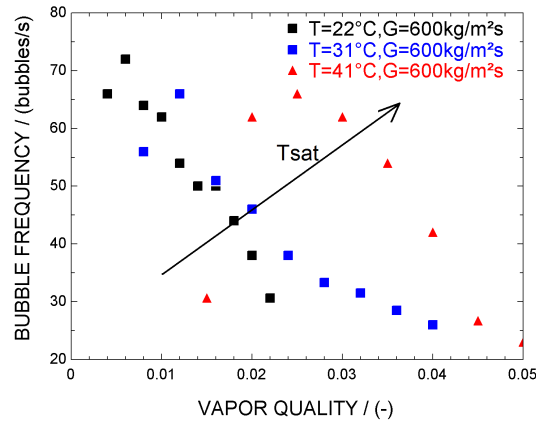


Figure 7. Illustration of the effect of the saturation temperature on the elongated bubble frequency.

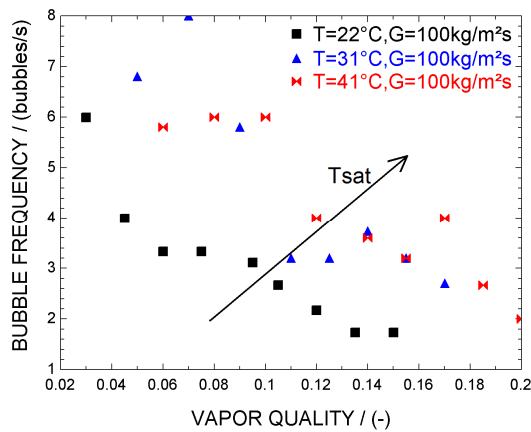


Figure 8. Illustration of the effect of the saturation temperature on the elongated bubble frequency.

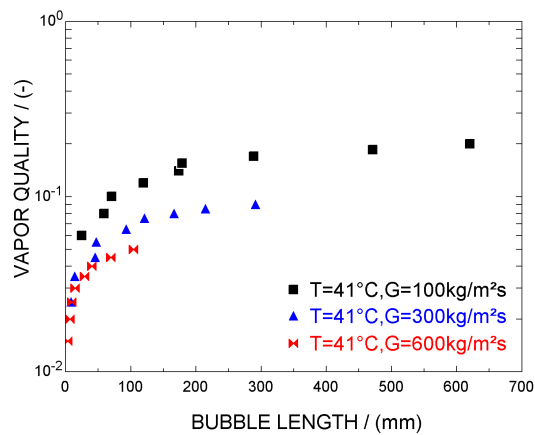


Figure 9. Illustration of the effect of the bubble length on the vapor quality.

4. CONCLUSIONS

A summary of the conclusions drawn from the results of the present experimental investigation on elongated bubble characteristic during flow boiling of R245fa in a micro-scale channel is as follows:

- a) The elongated bubble velocity increases with decreasing saturation temperature and increasing the vapor quality and mass velocity. The drift flux model with a new flow distribution parameter predicts satisfactorily the elongated bubble velocity.

- b) The elongated bubble frequency passes through a peak with increasing vapor quality from zero. The maximum bubble frequency moves to lower vapor qualities and has its value increased with increasing mass velocity.
- c) A vapor quality for the transition from elongated bubble to annular flow is indicated in a plot displaying vapor quality vs. elongated bubble length since as the bubble length increases up to “infinite” the vapor quality converges to a constant value.

5. ACKNOWLEDGEMENTS

The authors gratefully acknowledge the financial support under contract numbers 2005/60031-0, 2006/52089-1, 2008/10137-5 and 2008/10138-5 given by FAPESP (The State of São Paulo Research Foundation, Brazil). The technical support given to this investigation by Mr. José Roberto Bogno is also appreciated and deeply recognized.

6. REFERENCES

- Abernethy, R.B. and Thompson, J.W., 1973, *Handbook Uncertainty in Gas Turbine Measurements*, Arnold Engineering Development Center, Arnold Air Force Station, Tennessee.
- Agostini, B., Revellin, R. and Thome, J.R. 2008, “Elongated Bubbles in Microchannels. Part I: Experimental Study and Modeling of Elongated Bubble Velocity”, *Int. J. Mult. Flow*, Vol. 34, pp. 590-601.
- Arcanjo, A.A., Freitas, J.O., Tibiriça, C.B., Ribatski, G., 2009, “Two-Phase Flow Characteristics During Flow Boiling of Halocarbon Refrigerants in Micro-Scale Channels”, *Proceedings of the 7th ECI International Conference on Boiling Heat Transfer*, Florianópolis, Brasil, 2009.
- Consolini, L., Ribatski, G., Wei, Z., Xu J. and Thome, J.R., 2007 *Heat Transfer in Confined Forced Flow-Boiling*, *Heat Transfer Engineering*, Vol. 28, pp. 826-833.
- Felcar, H.O.M., Ribatski, G. and J.M. Saiz-Jabardo, 2007, “A Gas-Liquid Flow Pattern Predictive Method for Macro- and Mini-Scale Round Channels”, *Proceedings of the 10th UK Heat Transfer Conference*, Edinburgh, Scotland.
- Hetsroni, G., Mosyak, A., Pogrebnyak, E. and Segal, Z., 2005, “Explosive Boiling of Water in Parallel Micro-Channels”, *Int. J. Multiphase Flow*, Vol. 31, pp. 371-392.
- Moffat, R.J., 1988, “Describing the Uncertainties in Experimental Results”, *Exp. Thermal Fluid Sci.*, Vol. 1, pp. 3-17.
- Revellin, R. and Thome, J.R., 2007, “A New Type of Diabatic Flow Pattern Map for Boiling Heat Transfer in Microchannels”, *J. Micromech. Microeng.*, Vol. 17, pp. 788–796, 2007.
- Revellin, R., Agostini, B. and Thome, J.R., 2008a, “Elongated Bubbles in Microchannels. Part II: Experimental Study and Modeling of Bubble Collisions”, *Int. J. Mult. Flow*, Vol. 34, pp. 602-613.
- Revellin, R., Agostini, B. Ursenbacher, T. and Thome, J.R. 2008b “Experimental Investigation of Velocity and Length of Elongated Bubbles for Flow of R-134a in a 0.5 mm Microchannel”, *Exp. Thermal Fluid Science*, Vol. 32, pp. 870-881.
- Ribatski, G., Cabezas-Gómez, L., Navarro H.A. and Saiz-Jabardo, J.M., 2007, “The Advantages of Evaporation in Micro-Scale channels to Cool Microelectronic Devices”, *RETERM-Thermal Engineering*, Vol. 6, pp. 34-39.
- Zuber, N. and Findlay, J.A., 1965, “Average Volumetric Concentration in Two Phase Flow Systems”, *J. Heat Transfer*, Vol. 87, pp. 458–463.

7. RESPONSIBILITY NOTICE

The authors are the only responsible for the printed material included in this paper.